

# A Geometric Approach to Pairwise Bayesian Alignment of Functional Data Using Importance Sampling

Sebastian Kurtek

*Department of Statistics  
The Ohio State University  
Columbus, OH*

*e-mail:* [kurtek.1@stat.osu.edu](mailto:kurtek.1@stat.osu.edu)

**Abstract:** We present a Bayesian model for pairwise nonlinear registration of functional data. We utilize the geometry of the space of warping functions to define appropriate prior distributions and sample from the posterior using importance sampling. A simple square-root transformation is used to simplify the geometry of the space of warping functions, which allows for computation of sample statistics, such as the mean and median, and a fast implementation of a  $k$ -means clustering algorithm. These tools allow for efficient posterior inference, where multiple modes of the posterior distribution corresponding to multiple plausible alignments of the given functions are found. We also show pointwise 95% credible intervals to assess the uncertainty of the alignment in different clusters. We validate this model using simulations and present multiple examples on real data from different application domains including biometrics and medicine.

**MSC 2010 subject classifications:** Primary 62F15.

**Keywords and phrases:** functional data, warping function, Bayesian registration model, square-root slope function, square-root density.

## Contents

1	Introduction . . . . .	2
2	Problem Background . . . . .	4
2.1	Representation Space of Warping Functions . . . . .	6
3	Bayesian Registration Model . . . . .	8
4	Importance Sampling . . . . .	10
5	Simulation Studies . . . . .	12
5.1	Simulation 1 . . . . .	12
5.2	Simulation 2 . . . . .	14
6	Applications . . . . .	15
6.1	Biomedical Signals . . . . .	16
6.2	Berkeley Growth Velocity Data . . . . .	19
6.3	Signature Acceleration Functions . . . . .	20
6.4	Groupwise MAP Alignment to a Known Template . . . . .	22
7	Summary and Future Work . . . . .	23
	Acknowledgements . . . . .	25

References . . . . .	25
----------------------	----

## 1. Introduction

The problem of registration of functional data is important in many branches of science. In simple terms, it deals with deciding how points on one function match in some optimal way with points on another function. In contrast to landmark-based matching, such an approach matches the entire domains of the functions in a general registration problem. The study of registration problems is popular in image analysis where pixels or voxels across images are matched, and in shape analysis of objects where points across shapes are matched. One can broadly classify registration problems into two main groups: (1) pairwise registration and (2) groupwise registration. In pairwise registration, one solves for an optimal matching between two objects, while in groupwise registration multiple ( $> 2$ ) objects are simultaneously registered. In this paper, we focus on the problem of pairwise registration. This problem has been referred to in many different ways, some of which are alignment, warping, deformation matching, phase removal, and so on. While registration can be studied for many types of objects, from simple functions to complex high-dimensional objects, the fundamental issues in registration are often similar. We will focus on perhaps the simplest objects for studying registration problems,  $\mathbb{R}$ -valued functions on  $[0, 1]$ . More specifically, we will take a Bayesian approach to this problem, motivated by geometrical considerations; the method will be characterized by the definition of a geometric prior on a suitable function space, representing the parameter space of interest. We also compare the proposed method to past ideas that often take an optimization-based approach.

To motivate the function alignment problem, consider the example shown in Figure 1. In panel (a), we display an example of a PQRST complex with labeled structures (P wave, QRS complex, T wave). This function represents a full heartbeat cycle and is often extracted from long electrocardiogram (ECG) signals for the purposes of diagnosing heart diseases such as myocardial infarction. The difficulty with using such objects for diagnosis is highlighted in panel (b). As given, the P wave and QRS complex on the red function occur earlier than on the blue one. This is usually due to natural variability in nonlinear heartbeat dynamics. In general, given two PQRST complexes, their important salient features are often not in correspondence. This presents a major challenge when modeling these functions. Even simple statistics such as the cross-sectional mean can be meaningless. Aligning the functions prior to subsequent statistical analyses is thus required. The purpose of pairwise alignment is to estimate a warping function, and additionally the uncertainty in this estimate, that aligns the prominent features across two functions. In panel (c), we display the estimated warping function in red, and in panel (d) we show the resulting alignment of the two PQRST complexes. Now, the P wave, QRS complex and T wave occur at the same time across both functions.

There exists a large literature on statistical analysis of functions, in part due

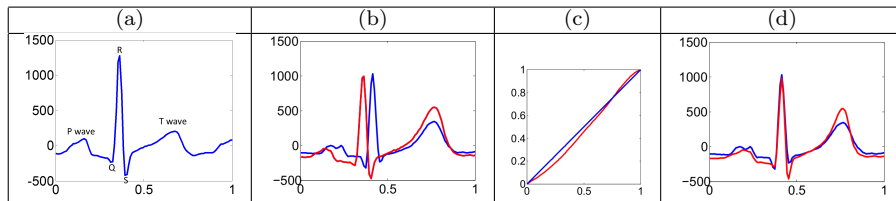


FIG 1. (a) A PQRST complex with labeled salient features: the P wave, QRS complex and T wave. (b) Two unaligned PQRST complexes. (c) The estimated warping function in red with no warping in blue as a reference. (d) The same PQRST complexes as in panel (b) but aligned using the estimated warping.

to the pioneering efforts of Ramsay and Kneip [22, 9], and several others [16, 29]. When restricting to the analysis of elastic functions (functions that are temporally aligned) the literature is relatively recent [21, 7, 16, 8, 29, 10, 19]. The general approach in most of these methods is to use an energy function to compute optimal registrations and perform subsequent analysis on the aligned functions using standard tools from functional data analysis such as the cross-sectional mean, covariance and functional Principal Component Analysis (fPCA).

Recently, it has been argued that a Bayesian approach rather than pure optimization is a better option for many situations. The advantages of a model-based Bayesian approach include:

1. A comprehensive exploration of the warping variable space resulting in potential multimodal solutions to the registration problem;
2. Assessment of uncertainty, via credible intervals, associated with the computed estimates.

The literature on registration methods that are based on Bayesian principles is fairly limited. Telesca and Inoue [30] proposed a semi-parametric model for groupwise alignment of functional data. These models were further extended in the context of analyzing microarray data in [31]. A nonparameteric approach to the groupwise registration problem was also proposed recently in [28]. A different Bayesian model was proposed for registering liquid chromatography-mass spectrometry data in [32]. The main difficulty in specifying Bayesian registration models lies in defining an appropriate prior on the space of warping functions, or some relevant subset, to enable efficient inference. The recent model of Cheng et al. [2] used the square-root slope function (SRSF) representation of functional data and utilized the fact that the derivative of a warping function is a probability density function. In this way, they constructed a Dirichlet process to impose a prior model implicitly on the space of warping functions, and sampled from the posterior distribution using Markov Chain Monte Carlo techniques. The SRSF representation of functional data has many desirable properties related to the registration problem, which we emphasize in Section 2.

In the current paper, we describe a very convenient geometric structure, a unit sphere, using the square-root density (SRD) representation of warping

functions and use its geometry to impose priors on high-dimensional spheres. In this setup, we develop a Bayesian registration model and utilize importance sampling to sample from the posterior and compute posterior functionals such as the mean, median or maximum a posteriori probability (MAP) estimate. We also provide pointwise standard deviations and credible intervals to assess alignment uncertainty. We show that these tools are especially effective when two or more registrations are plausible. We note that the spherical geometry of the space of warping functions in conjunction with importance sampling has not been previously explored for Bayesian alignment of functional data. Furthermore, the approaches in current literature are not directly concerned with defining multiple plausible function alignments using different modes of the posterior distribution.

The rest of this paper is organized as follows. In Section 2, we give a detailed description of the registration problem and describe tools for statistical analysis on the space of warping functions. In Section 3, we introduce our registration model and in Section 4 we describe an importance sampling approach for sampling from the posterior distribution of warping functions. Finally, in Sections 5 and 6, we present simulation studies and different applications of the proposed framework. We emphasize examples where the posterior distribution is multi-modal. Finally, we close with a brief summary and directions for future work in Section 7.

## 2. Problem Background

Before we describe our Bayesian framework, we first setup the registration problem mathematically. Let  $\mathcal{F}$  be an appropriate subset (made precise later) of real-valued functions on the interval  $[0, 1]$ . For any two functions  $f_1, f_2 \in \mathcal{F}$ , the registration problem is defined as finding the mapping  $\gamma$  such that point  $t \in [0, 1]$  in the domain of  $f_1$  is matched to the point  $\gamma(t)$  in the domain of  $f_2$ . In other words, the functions  $f_1(t)$  and  $f_2(\gamma(t))$  are optimally matched under the chosen optimality criterion. The main question that arises is: What should be the criterion for optimal registration? A natural tendency is to choose an  $\mathbb{L}^p$ -norm between  $f_1$  and  $f_2 \circ \gamma$ , but there are some known limitations of that approach. For instance, if we choose the  $\mathbb{L}^2$  norm, defined as  $\|f_1 - f_2\| = \sqrt{\int_0^1 |f_1(t) - f_2(t)|^2 dt}$ , we obtain the following optimization problem:

$$\gamma^* = \arg \inf_{\gamma} \|f_1 - f_2 \circ \gamma\|. \quad (1)$$

This setup can lead to a degenerate solution, termed the *pinching effect*. In this case, one can pinch the entire function  $f_2$  to get arbitrarily close to  $f_1$  in  $\mathbb{L}^2$  norm. To avoid this situation, one often adds a roughness penalty on  $\gamma$ , denoted by  $\mathcal{R}(\gamma)$ , leading to the optimization problem  $\inf_{\gamma} (\|f_1 - f_2 \circ \gamma\|^2 + \lambda \mathcal{R}(\gamma))$ . Although this avoids the pinching effect, it introduces some other issues. First, the choice of  $\lambda$  is not obvious in general cases. Second and more important is the fact that this solution is not symmetric. That is, the optimal registration of  $f_1$

to  $f_2$  can be quite different from that of  $f_2$  to  $f_1$ . Another related issue is that this criterion is not a proper metric and this leads to additional problems in later analysis. Most papers on registration of functional data involve this setup and inherit the above-mentioned limitations.

In order to handle these issues, Srivastava et al. [27, 12] proposed a novel approach that has its foundations in differential geometry. First, let the set of all registration or warping functions be defined as  $\Gamma = \{\gamma : [0, 1] \rightarrow [0, 1] | \gamma(0) = 0, \gamma(1) = 1, 0 < \dot{\gamma} < \infty\}$ .  $\Gamma$  forms a Lie group under composition, i.e., for any  $\gamma_1, \gamma_2 \in \Gamma$  their composition  $\gamma_1 \circ \gamma_2$  is also in  $\Gamma$ , and for any  $\gamma \in \Gamma$  there is a unique  $\gamma^{-1} \in \Gamma$ . The  $\gamma_{id}(t) = t$  is the identity element of this group. The next item is to represent the given functions by their square-root slope functions (SRSFs):  $q(t) = \text{sign}(\dot{f}(t))\sqrt{|\dot{f}(t)|}$ . For registration analysis in this approach, each  $f \in \mathcal{F}$  is represented by its SRSF  $q$ . One sets  $\mathcal{F}$  to be the space of all absolutely continuous functions and the resulting space of all SRSFs is  $\mathbb{L}^2([0, 1], \mathbb{R})$  henceforth referred to simply as  $\mathbb{L}^2$ . For every  $q \in \mathbb{L}^2$  there exists a function  $f$  (unique up to a constant) such that the given  $q$  is the SRSF of that  $f$ . In fact, this function can be obtained precisely using the equation  $f(t) = f(0) + \int_0^t q(s)|q(s)|ds$ . Note that if a function  $f$  is warped by  $\gamma$  to  $f \circ \gamma$ , its SRSF changes from  $q$  to  $(q, \gamma) = (q \circ \gamma)\sqrt{\dot{\gamma}}$ ; this last term involving  $\sqrt{\dot{\gamma}}$  is an important departure from previous solutions. To setup the registration problem, we define an equivalence class of an SRSF as  $[q] = \{(q, \gamma) | \gamma \in \Gamma\}$ . Finally, the pairwise registration between any two functions  $f_1$  and  $f_2$  is performed by solving an optimization problem over equivalence classes of their SRSF representations:

$$\gamma_{DP} = \arg \inf_{\gamma \in \Gamma} \|q_1 - (q_2, \gamma)\|. \quad (2)$$

The solution to this problem is computed using the dynamic programming (DP) algorithm. The resulting distance between the aligned  $f_1$  and  $f_2$  is given by:

$$d([q_1], [q_2]) = \|q_1 - (q_2, \gamma_{DP})\|. \quad (3)$$

As described in [27], this framework has many advances: it avoids the pinching problem, its registration solution is symmetric, it does not require an additional regularization term and the choice of  $\lambda$  that goes with it, and it is actually a proper metric in the quotient space  $\mathcal{F}/\Gamma$ , which provides an important tool for ensuing analysis. The most important reason why this setup avoids many problems of Equation 1 is that  $\|q_1 - q_2\| = \|(q_1, \gamma) - (q_2, \gamma)\|$  for any  $\gamma \in \Gamma$ . In mathematical terms, it means that the action of  $\Gamma$  on  $\mathbb{L}^2$  is by isometries. The original method was later extended to apply to statistical analysis of cyclostationary biosignals [14], and was shown to perform well in different applications [33, 34, 37, 18].

While the framework of Srivastava et al. [27] is precise in mathematically defining the function registration problem, it solves for optimal warping functions via energy optimization. In this paper, we argue that a model-based Bayesian approach has many additional advantages. Thus, to preserve the nice properties, such as the isometric action of  $\Gamma$  under  $\mathbb{L}^2$  metric, we build our Bayesian model using the SRSF representation of functional data.

### 2.1. Representation Space of Warping Functions

The proposed Bayesian model utilizes prior distributions and importance functions on the space of warping functions,  $\Gamma$ . Thus, we are faced with defining statistics and probability distributions on this space. In order to do this we use the Fisher-Rao Riemannian metric on  $\Gamma$ , which is given by (for  $w_1, w_2 \in T_\gamma(\Gamma)$  and  $\gamma \in \Gamma$ )  $\langle\langle w_1, w_2 \rangle\rangle_\gamma = \int_0^1 \dot{w}_1(t) \dot{w}_2(t) \frac{1}{\dot{\gamma}(t)} dt$  [25, 26, 11], where  $\dot{w}$  and  $\dot{\gamma}$  represent time derivatives. An important property of the Fisher-Rao metric is that it is invariant to re-parameterizations of probability density functions [36]. While this is not the only metric that achieves this property, it is important to note that there is no invariant metric that does not include derivatives. It is possible to define statistics and probability models directly on  $\Gamma$  under the Fisher-Rao metric, but this proves to be very complicated due to the non-trivial Riemannian geometry of this space. We use the Fisher-Rao Riemannian geometry in our Bayesian setup because the desirable properties of this metric (i.e., parameterization invariance) will naturally translate to the prior distributions on  $\Gamma$ .

Inference on  $\Gamma$  is greatly simplified using a convenient transformation, which is similar to the definition of the SRSF for general functions [1].

**Definition 1.** Define the mapping  $\phi : \Gamma \rightarrow \Psi$ . Then, given an element  $\gamma \in \Gamma$ , define a new representation  $\psi : [0, 1] \rightarrow \mathbb{R}_{>0}$  using the square-root of its derivative as  $\phi(\gamma) = \psi = \sqrt{\dot{\gamma}}$ .

This is the same as the SRSF defined earlier for functions and takes this form because  $\dot{\gamma} > 0 \forall t$ . For simplicity and to distinguish it from the SRSF representation of functions, we refer to this representation as the square-root density (SRD). The identity map  $\gamma_{id}(t) = t$  maps to a constant function with value  $\psi_{id}(t) = 1$ . An important advantage of this transformation is that the  $\mathbb{L}^2$  norm of a function  $\psi$  is 1, i.e.,  $\|\psi\|^2 = \int_0^1 \psi(t)^2 dt = \int_0^1 \dot{\gamma}(t) dt = \gamma(1) - \gamma(0) = 1$ . Thus, the set of all such  $\psi$ s, denoted by  $\Psi$ , is a subset of the unit sphere in  $\mathbb{L}^2$ . The tangent space for all  $\psi$  that are not on the boundary of  $\Psi$  is defined as  $T_\psi(\Psi) = \{v : [0, 1] \rightarrow \mathbb{R} | \langle v, \psi \rangle = 0\}$ , where  $\langle \cdot, \cdot \rangle$  is the standard  $\mathbb{L}^2$  inner product. Furthermore, as shown in [1, 25, 26, 11], the Fisher-Rao metric on the space of warping functions simplifies to the  $\mathbb{L}^2$  metric on  $\Psi$ , which in turn greatly simplifies all computation. Given a function  $\psi$  one can easily compute the corresponding warping function via integration using  $\gamma(t) = \int_0^t \psi(s)^2 ds$ ; this provides the inverse mapping  $\phi^{-1} : \Psi \rightarrow \Gamma$ . Thus, the geodesic path between two warping functions,  $\gamma_1, \gamma_2 \in \Gamma$  represented using their SRDs  $\psi_1, \psi_2 \in \Psi$ , is simply the great circle connecting them ( $\alpha : [0, 1] \rightarrow \Psi$ ),  $\alpha(\tau) = \frac{1}{\sin(\theta)} [\sin(\theta - \theta\tau)\psi_1 + \sin(\theta\tau)\psi_2]$ , where  $\theta$  represents the length of this path (geodesic distance between warping functions  $\gamma_1$  and  $\gamma_2$  under the Fisher-Rao metric) and is simply the arc-length between  $\psi_1$  and  $\psi_2$ :

$$d(\gamma_1, \gamma_2)_{FR} = d(\psi_1, \psi_2) = \theta = \cos^{-1}(\langle \psi_1, \psi_2 \rangle). \quad (4)$$

Since the differential geometry of the sphere is well known, this transformation also simplifies the problem of defining probability distributions of warping

functions. The general approach will be to define wrapped probability distributions, and perform random sampling and probability calculations on  $\Psi$ . In order to achieve this goal, we must first define some standard tools from differential geometry for this space. We begin by providing the definition of the exponential and inverse exponential maps. For  $\psi \in \Psi$  and  $v \in T_\psi(\Psi)$ , the exponential map is defined as  $\exp : T_\psi(\Psi) \rightarrow \Psi$  by  $\exp_\psi(v) = \cos(\|v\|)\psi + \frac{\sin(\|v\|)}{\|v\|}v$ . For  $\psi_1, \psi_2 \in \Psi$ , the inverse exponential map is defined as  $\exp^{-1} : \Psi \rightarrow T_\psi(\Psi)$  by  $\exp_{\psi_1}^{-1}(\psi_2) = \frac{\theta}{\sin(\theta)}(\psi_2 - \cos(\theta)\psi_1)$ . These two expressions provide a natural way of mapping points from the representation space  $\Psi$  to the tangent space (at a particular element of  $\Psi$ ) and vice versa. Another tool from differential geometry that is useful in defining probability models on the space of warping functions is parallel transport. This tool transports tangent vectors along paths on a Riemannian manifold. We use the parallel transport along geodesic paths (in this case great circles on the sphere) to define an orthonormal basis in the tangent space at any point on  $\Psi$  by transporting a standard basis defined on the tangent space at the identity element,  $T_1(\Psi)$ . For  $\psi_1, \psi_2 \in \Psi$ , the shortest geodesic path  $\alpha : [0, 1] \rightarrow \Psi$  such that  $\alpha(0) = \psi_1$  and  $\alpha(1) = \psi_2$ , and a vector  $v \in T_{\psi_1}(\Psi)$ , its parallel transport along  $\alpha$  to  $\psi_2$  is defined as  $w = v - \frac{2\langle v, \psi_2 \rangle}{\|\psi_1 + \psi_2\|}(\psi_1 + \psi_2)$ . This defines a mapping  $\kappa : T_{\psi_1}(\Psi) \rightarrow T_{\psi_2}(\Psi)$  such that  $w = \kappa(v)$ . An important property of parallel transport is that the mapping  $\kappa$  is an isometry between the two tangent spaces, i.e., for  $v_1, v_2 \in T_{\psi_1}(\Psi)$ ,  $\langle v_1, v_2 \rangle = \langle \kappa(v_1), \kappa(v_2) \rangle$ .

**Summary Statistics on  $\Psi$ :** In addition to defining prior distributions on the space of warping functions, we would like to be able to compute summary statistics such as the mean or median. These tools are especially useful in inference based on samples generated from the posterior distribution. Suppose that we have a sample of warping functions  $\gamma_1, \dots, \gamma_p$ . To begin, we are interested in defining a mean and median of these functions. To do this we again exploit the geometry of  $\Psi$ . We begin by mapping all of the functions  $\gamma$  to their corresponding SRD representations resulting in  $\psi_1, \dots, \psi_p$ . Once this is done, all of our data is on the subset of the unit sphere, where the geodesic distance is used to compute their intrinsic mean and median as follows. The sample Karcher mean is given by  $\bar{\psi} = \operatorname{argmin}_{\psi \in \Psi} \sum_{i=1}^p d(\psi, \psi_i)^2$  while the sample geometric median is defined as  $\tilde{\psi} = \operatorname{argmin}_{\psi \in \Psi} \sum_{i=1}^p d(\psi, \psi_i)$ . Gradient-based approaches for finding the Karcher mean and geometric median are given in several places [15, 5, 6, 13] and are omitted here for brevity.

**K-means Clustering on  $\Psi$ :** One of the motivations behind this work is the discovery and analysis of multiple modes in the posterior distribution of warping functions. For this purpose, we introduce a  $k$ -means clustering approach on  $\Psi$ . In the previous section, we have defined a procedure to compute the Karcher mean of warping functions and we will use it to specify the  $k$ -means clustering algorithm. Let  $\gamma_1, \dots, \gamma_p$  be a sample from the posterior distribution and  $\psi_1, \dots, \psi_p$  be their corresponding SRD representations. The  $k$ -means clustering approach computes a partition of the sample space such that the within cluster sum of squared distances is minimized. This is achieved using the following standard algorithm [17]:



**Algorithm 1. (*k*-Means):** Initialize using  $k$  unique functions  $\bar{\psi}_{1,0}, \dots, \bar{\psi}_{k,0}$  as cluster centers and set  $j = 0$ .

(1) For each  $i = 1, \dots, p$  and  $m = 1, \dots, k$ , compute  $d_{i,m} = d(\bar{\psi}_{m,j}, \psi_i)$  using Equation 4.

(2) Assign each function  $\psi_i$ ,  $i = 1, \dots, p$ , to the cluster which minimizes  $d_{i,\cdot}$ .

(3) Update cluster means  $\bar{\psi}_{1,j+1}, \dots, \bar{\psi}_{k,j+1}$  using the Karcher mean.

(4) Set  $j = j + 1$ .

(5) Repeat Steps 1-4 until cluster assignments remain unchanged.

A major benefit of this algorithm is its flexibility. One can easily replace the  $k$ -means formulation by, for example,  $k$ -medians. This is especially useful when the mean may not be a good estimate of the posterior mode of interest.

There are two main limitations of this algorithm: (1) the solution strongly depends on the initialization of the  $k$  cluster means, and (2) the number of clusters  $k$  must be specified a priori (usually the expected number of posterior modes is unknown). We address the first issue using hierarchical distance-based clustering as follows. First, we compute all pairwise distances between the given samples using Equation 4 and perform hierarchical clustering using the maximum linkage criterion. We then initialize the  $k$ -means clustering algorithm using the  $k$  clusters provided by hierarchical clustering. To address the second issue, we use the following procedure to determine the “correct” number of clusters or posterior modes  $k$ . First, we compute the pooled total variance across all clusters for  $k = 1$  and  $k = 2$ . To decide whether the posterior has multiple modes we examine the percentage decrease in the pooled variance due to the additional second cluster. If the percentage decrease is greater than 30%, we proceed to cluster the posterior samples. While this cutoff value seems ad-hoc, we have found through many simulations and real data examples that it works well in practice. Then, to decide on the final number of clusters, we use the silhouette measure of Rousseeuw [23].

**Discretization:** In order to apply the proposed methodology we discretize the functional data and the warping functions using a dense sampling of  $N$  points:  $t = \{t_1, \dots, t_N\} \in [0, 1]^N$ , where  $N$  depends on the application of interest. We study the effects of changing  $N$  on the final inference results in Section 5.1. This allows us to model differences between SRSFs using multivariate Gaussian distributions, and to define prior probability models on the space of warping functions using multivariate wrapped Gaussian distributions. In addition, we use discrete approximations to compute the quantities defined in Section 2.

### 3. Bayesian Registration Model

Given two functions  $f_1, f_2$  and their corresponding SRSFs  $q_1, q_2$ , we introduce a novel Bayesian model for function registration. To begin, we re-scale the functions such that  $\|q\| = 1$ , i.e., all SRSFs lie on the unit sphere. As shown in [27], a major benefit of the metric introduced in Section 2 is that estimating  $\gamma$  is independent of amplitude scales of the given functions. Re-scaling the func-



tions improves computational stability and allows us to specify a simpler prior model for the standard deviation in the likelihood. At the first stage, we model the difference  $q_1 - (q_2 \circ \phi^{-1}(\psi))\psi|\psi$  using a zero-mean Gaussian process. This part of our model is exactly the same as that proposed in [2]. The motivation behind this likelihood function is to model the pointwise deviations of the two functions being aligned (sampled at the same time points) using a zero-mean, multivariate Gaussian distribution after discretization. While other likelihoods are also possible, this is a reasonable choice that works well in practice. That is,

$$q_1 - (q_2 \circ \phi^{-1}(\psi))\psi|\psi, \sigma_1 \sim N(0, \sigma_1^2 I_N) \text{ (likelihood denoted by } L), \quad (5)$$

where  $N$  denotes the number of points sampled on the two functions.

The second stage of our model places a truncated wrapped normal (TWN) prior distribution on the space of time warping functions  $\Gamma$  by utilizing their SRD representation:

$$\psi \sim TWN(\mu_\psi, \Sigma_\psi) \text{ (denoted by } \pi_\psi). \quad (6)$$

We set the mean of the prior to be the identity mapping  $\mu_\psi = 1$ , which provides natural regularization toward  $\gamma_{id}$  (i.e., no warping). We also truncate the support of the prior using half of the maximum distance on  $\Psi$ ,  $\pi/4$ . One can show that this truncation ensures positive mass only on the subset of the sphere containing valid warping functions (in the discretized case). Thus, the prior distribution  $\pi$  is a truncated wrapped Gaussian distribution defined and evaluated in  $T_1(\Psi)$ . This definition is similar to that presented in Kurtek et al. [11]; an alternative construction of Gaussian distributions on high-dimensional spheres is given in [4].

To define the covariance structure, we require an orthonormal basis in the tangent space  $T_1(\Psi)$ . We begin by defining a set of basis elements, which are orthogonal to the representation space and have  $\mathbb{L}^2$  norm 1:  $\tilde{B}_1 = \{\sqrt{3}(1 - 2t), \sqrt{2}\sin(2\pi jt), \sqrt{2}\cos(2\pi jt) | j = 1, 2, \dots, n\}$ . Then, to form an orthonormal basis for the tangent space  $T_1(\Psi)$ , we utilize the Gramm-Schmidt procedure under the  $\mathbb{L}^2$  metric. Notice that this orthonormal basis, denoted by  $\tilde{B}$ , is truncated by choosing a maximum number  $j = n$ , which yields  $2n + 1$  basis elements. The truncation of the basis is important for additional regularization (smoothness of the warping functions) and computational efficiency. This, in turn, enables us to define a diagonal covariance matrix in terms of the basis as  $\Sigma_\psi = \tilde{B}^T K_1 \tilde{B}$ , where  $K_1$  is a diagonal covariance matrix with entries  $\sigma_2^2/j^4$  as the  $j$ th diagonal elements, with a large value for  $\sigma_2^2$ . Thus, we assume a non-informative prior distribution on the directions given by the basis  $\tilde{B}$ . We choose quadratic decay of the standard deviation with respect to the degree of the basis functions based on simulations presented in Section 5.1. We require at least a linear decay for the eigenvalues of the covariance operator to be summable [3]. In practice, we want to favor smoother warping functions; thus, we weigh the low frequency basis elements (corresponding to low values of  $j$ ) higher than the high frequency basis elements. Note that the standard deviation of the additional linear basis element is not penalized. The truncated wrapped normal prior is then defined

as follows:

$$\pi_\psi(\psi|1, K_1) \propto \exp\left(-\frac{1}{2} \exp_1^{-1}(\psi) \tilde{B}^T K_1^{-1} \tilde{B} \exp_1^{-1}(\psi)^T\right) I_{\{\|\exp_1^{-1}(\psi)\| \leq \pi/4\}}, \quad (7)$$

where  $I$  is the indicator function.

Due to the unit  $\mathbb{L}^2$  norm constraint on the re-scaled SRSFs of the functions to be aligned, the maximum distance between them is  $\pi$ , i.e., the maximum distance on a unit sphere. Thus, we put a uniform prior model on  $\sigma_1$  with parameters 0 and  $\pi/2$ ; this prior is denoted by  $\pi_{\sigma_1}$ . We assume that the registration variable,  $\psi$ , and the standard deviation in the likelihood,  $\sigma_1$ , are independent. This is a reasonable assumption due to the fact that the alignment of two functions does not depend on their scale, as mentioned earlier.

Under this specification of the model, the posterior distribution of  $\psi$  becomes:

$$f(\psi|q_1, q_2) \propto \int_0^{\pi/2} L(q_1 - (q_2 \circ \phi^{-1}(\psi))\psi|\psi, \sigma_1) \pi_\psi(\psi) \pi_{\sigma_1}(\sigma_1) d\sigma_1. \quad (8)$$

In order to sample from the posterior distribution and perform Bayesian inference we will utilize importance sampling on  $\Psi$ .

#### 4. Importance Sampling

We begin by briefly introducing the concept of importance sampling and then provide some details of how this can be applied to our problem. Importance sampling is a variance reduction technique in Monte Carlo estimation where instead of directly sampling from a distribution of interest, which may be inefficient, one first samples from an importance function and then re-samples based on appropriate weights. Suppose that we are interested in estimating the value of the following integral:  $\theta = \int_{\mathcal{X}} g(x) f(x) dx$ , where  $f(x)$  is a probability density function. The classical Monte Carlo estimate of this integral is given by  $\hat{\theta} = \sum_{i=1}^S g(x_i)$ , where  $\{x_1, \dots, x_S\}$  are *iid* samples from  $f$ . If the variance of the classical Monte Carlo estimate is large it may be beneficial to introduce a new function  $h$ , termed the *importance function*, which can be used to generate the samples instead of  $f$ . One can then rewrite the integral as  $\theta = \int_{\mathcal{X}} \frac{g(x)f(x)}{h(x)} h(x) dx$ . The improved Monte Carlo estimate becomes  $\tilde{\theta} = \sum_{i=1}^S g(x_i) w(x_i)$ , where  $\{x_1, \dots, x_S\}$  are *iid* samples from  $h$  and  $w(x) = \frac{f(x)}{h(x)}$ . We use this idea to generate samples from the posterior distribution represented by  $f$  as follows. Given a large sample  $\{x_1, \dots, x_S\}$  from  $h$ , we compute the associated weights as  $\{\frac{f(x_1)}{h(x_1)}, \dots, \frac{f(x_S)}{h(x_S)}\}$ . Then, to obtain  $s$  samples from  $f$  (where  $s$  is generally much smaller than  $S$ ), we re-sample the set  $\{x_1, \dots, x_S\}$  with the corresponding (normalized) weights. This provides a flexible and efficient methodology for sampling from the posterior distribution. This process is also called sampling importance re-sampling. In the current work, we use an improved method for sampling importance re-sampling without replacement given in [24].

For our problem, we are faced with defining an importance function  $h$  that allows us to efficiently sample from  $f$ . The main requirement on  $h$  is that its support is the same as  $f$ . One option is to use the prior as the importance function directly, and generate the weights using the likelihood. But, in other cases, one may want to “upsample” a different part of the space, e.g., near the dynamic programming solution. Thus, we provide a general recipe for constructing wrapped Gaussian importance functions similar to the definition of the prior.

In order to do this, we require a method for defining an orthonormal basis in the tangent space at any point on  $\Psi$ . Given the truncated basis  $\tilde{B}$  in  $T_1(\Psi)$  defined in the previous section, we can define an orthonormal basis in the tangent space at an arbitrary point  $T_{\mu_\psi}(\Psi)$  using parallel transport, which was defined in Section 2.1. Parallel transport defines an isometric mapping between tangent spaces, and thus preserves the lengths of the basis vectors and the angles between them. We refer to the orthonormal basis in  $T_{\mu_\psi}(\Psi)$  as  $B$  and use it to define a coordinate system in that space. This, in turn, enables us to define the covariance matrix as  $\Sigma_\psi = B^T K B$ , where  $K$  is diagonal with  $\sigma_3^2/j^4$  as its  $j$ th diagonal element. In this way we can define a general version of the importance function as

$$h(\psi|\mu_\psi, K) \propto \exp\left(-\frac{1}{2} \exp_{\mu_\psi}^{-1}(\psi) B^T K^{-1} B \exp_{\mu_\psi}^{-1}(\psi)^T\right). \quad (9)$$

Note that there is no need to truncate the importance function. Figure 2 provides a pictorial explanation of our definition of the wrapped normal importance function in the tangent space. Given this setup, we can generate random samples from  $h$  in the tangent space using  $v_{rnd} = \sum_{j=1}^{2n} z_j \sqrt{K_{jj}} B_j$  where  $z_j \stackrel{iid}{\sim} N(0, 1)$ .  $B_j$  denotes the  $j$ th row of  $B$  ( $j$ th basis element) and  $K_{jj}$  denotes the  $j$ th diagonal element of the matrix  $K$ .  $v_{rnd}$  can be mapped to  $\Psi$  using  $\psi_{rnd} = \exp_{\mu_\psi}(v_{rnd})$ .

Using the idea of importance sampling, we can re-write the posterior distribution as follows:

$$f(\psi|q_1, q_2) \propto \int_0^{\frac{\pi}{2}} \frac{L(q_1 - (q_2 \circ \phi^{-1}(\psi))\psi|\psi, \sigma_1) \pi_\psi(\psi) \pi_{\sigma_1}(\sigma_1) h(\psi)}{h(\psi)} d\sigma_1. \quad (10)$$

Note that it is obvious from the expression in Equation 10, that in the special case when the importance function is the same as the prior, one can simply sample from the prior distribution and weight each sample using the likelihood (after integrating out  $\sigma_1$ ).

Thus, our approach is to generate a large sample  $\{\psi_1, \dots, \psi_S\}$  from  $h$  and evaluate a weight for each sampled warping function using:

$$\begin{aligned} \eta_i &= \int_0^{\frac{\pi}{2}} \frac{L(q_1 - (q_2 \circ \phi^{-1}(\psi_i))\psi_i|\psi_i, \sigma_1) \pi_\psi(\psi_i) \pi_{\sigma_1}(\sigma_1)}{h(\psi_i)} d\sigma_1 \\ &\propto \int_0^{\frac{\pi}{2}} \sigma_1^{-(N-1)} \exp\left(-\frac{1}{2\sigma_1^2} \|q_1 - (q_2 \circ \psi^{-1}(\psi_i))\psi_i\|^2\right. \\ &\quad \left.- \frac{1}{2} \exp_1^{-1}(\psi) \tilde{B}^T K_1^{-1} \tilde{B} \exp_1^{-1}(\psi)^T\right. \\ &\quad \left.+ \frac{1}{2} \exp_{\mu_\psi}^{-1}(\psi) B^T K^{-1} B \exp_{\mu_\psi}^{-1}(\psi)^T\right) I_{\{\|\exp_1^{-1}(\psi)\| \leq \pi/4\}} d\sigma_1, \quad i = 1, \dots, S. \end{aligned}$$

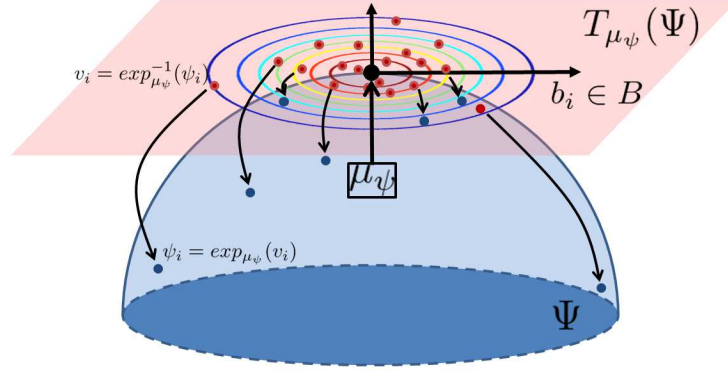


FIG 2. We define wrapped normal densities in the tangent space at a pre-specified mean. We utilize these models as and importance functions on the space of warping functions. One can generate random samples from the Gaussian model on the tangent space and then use the exponential map to get a random warping function.

Once all of the weights have been computed, we re-sample a small number  $s$  of  $\psi$ s from the original set using the methods proposed in [24]. The re-sampled functions  $\psi_1, \dots, \psi_s$  are samples from the posterior distribution  $f$ , and can be mapped to their corresponding warping functions using  $\phi^{-1}$ . Posterior functionals can be mapped to  $\Gamma$  in the same way.

## 5. Simulation Studies

In this section, we present warping results using simulated scenarios. In all examples, we fix the original sample size to  $S = 500000$ , the posterior sample size to  $s = 200$ , and the number of basis elements in the prior and importance function to  $N - 1$ , where  $N$  is the sampling density of the given functions. The importance function used throughout the simulation studies and the real applications is a wrapped Gaussian centered at the identity element with the same covariance structure as the prior.

### 5.1. Simulation 1

In the first simulation study, we consider the effects of function sampling density and the order of decay of the standard deviation in the prior distribution. For this purpose, we have simulated three different warping functions,  $\gamma_1 = t + 0.15t(1-t)$ ,  $\gamma_2 = t + 0.70t(1-t)$ ,  $\gamma_3 = t + 0.1 \sin(2\pi t)$ ,  $t = [0, 1]$ , and applied them to a function with two modes denoted by  $f$ . We display the original function  $f$  in Figure 3(a) in blue and the same function under the three warpings,  $f \circ \gamma_1$ ,  $f \circ \gamma_2$  and  $f \circ \gamma_3$ , in red, green and black, respectively.

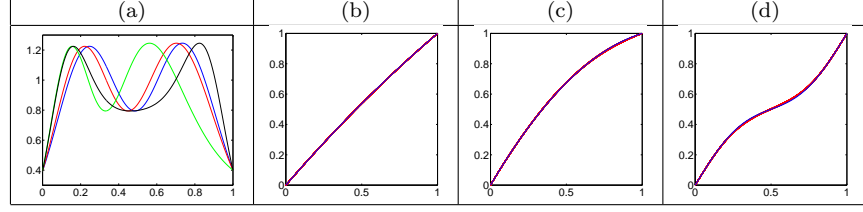


FIG 3. (a) Simulated data with  $f$  in blue,  $f \circ \gamma_1$  in red,  $f \circ \gamma_2$  in green, and  $f \circ \gamma_3$  in black. (b)-(d) True warpings  $\gamma_1$ ,  $\gamma_2$  and  $\gamma_3$  in blue, respectively, with 100 posterior means in red.

TABLE 1

Simulation results for correct warping recovery for three different warping functions and sampling densities (SD) under quadratic decay of the prior standard deviations. (a) Average  $d_{FR}(\gamma_T, \bar{\gamma})$  with the standard deviations in parentheses ( $T=$ true). (b)  $d_{FR}(\gamma_T, \gamma_{DP})$ . (c) Average  $d_{FR}(\gamma_T, \bar{\gamma}_{DIR})$  with the standard deviations in parentheses. (d) Average  $DPD_{PM}$  ( $PM=$ proposed method). (e)  $DPD_{DP}$ . (f) Average  $DPD_{DIR}$ . Best results are in bold.

Ex.	SD	(a)	(b)	(c)	(d)	(e)	(f)
$\gamma_1$	50	<b>0.0055 (0.0007)</b>	0.0359	-	<b>95.6</b>	85.4	-
	100	<b>0.0018 (0.0005)</b>	0.0366	0.0206 (0.0022)	<b>98.3</b>	88.3	89.3
	150	<b>0.0017 (0.0006)</b>	0.0384	-	<b>97.5</b>	88.8	-
$\gamma_2$	50	<b>0.0118 (0.0026)</b>	0.0312	-	<b>98.3</b>	96.5	-
	100	<b>0.0125 (0.0030)</b>	0.0211	0.0443 (0.0032)	<b>98.3</b>	98.1	87.4
	150	<b>0.0127 (0.0028)</b>	0.0182	-	96.9	<b>98.3</b>	-
$\gamma_3$	50	<b>0.0235 (0.0026)</b>	0.0284	-	<b>96.0</b>	95.9	-
	100	0.0257 (0.0027)	<b>0.0212</b>	0.0727 (0.0037)	94.9	<b>97.0</b>	93.1
	150	0.0257 (0.0027)	<b>0.0192</b>	-	93.4	<b>97.1</b>	-

We apply the proposed model to perform pairwise Bayesian alignment for each example using 100 replicates, and report the detailed results in Table 1 for quadratic decay of the prior standard deviations and sampling densities of 50, 100 and 150 points. For each example, we report the average Fisher–Rao distance between the true warping function and the estimated posterior mean  $\bar{\gamma}$  in panel (a), the Fisher–Rao distance between the true warping function and the dynamic programming solution  $\gamma_{DP}$  in panel (b), and the average Fisher–Rao distance between the true warping function and the estimated posterior mean when using a Dirichlet prior  $\bar{\gamma}_{DIR}$  in panel (c). In all of the presented results, we set the parameters of the Dirichlet distribution to  $\alpha_1 = \dots = \alpha_{40} = 1$ , and use importance sampling to sample from the posterior. The standard deviations of the distances are also provided in parentheses. We highlight the best performance for each example and sampling density in bold. In all examples, the proposed geometric Bayesian model outperforms a model with a Dirichlet prior on the warping functions (i.e., the model of Cheng et al. [2]). Furthermore, the performance of the proposed method is comparable to, and often better than, the commonly used dynamic programming algorithm. In panels (d)–(f), we report the average percentage decrease in the distance between the two functions being registered, i.e.,  $DPD = \frac{\|q_1 - q_2\| - \|q_1 - (q_2, \gamma)\|}{\|q_1 - q_2\|}$ . Again, the proposed model

TABLE 2

Simulation results for correct warping recovery for three different warping functions and sampling densities (SD) under linear and no decay of the prior standard deviations. (a) Average  $d_{FR}(\gamma_T, \hat{\gamma})$  with the standard deviations in parentheses ( $T=\text{true}$ ). (b) Average  $DPD_{PM}$  ( $PM=\text{proposed method}$ ).

Ex.	SD	Linear Decay		No Decay	
		(a)	(b)	(a)	(b)
$\gamma_1$	50	0.0060 (0.0007)	95.7	-	-
	100	0.0027 (0.0007)	97.8	0.0088 (0.0008)	90.3
	150	0.0029 (0.0007)	97.5	-	-
$\gamma_2$	50	0.0167 (0.0035)	97.3	-	-
	100	0.0197 (0.0032)	97.4	0.0562 (0.0029)	91.4
	150	0.0203 (0.0033)	96.9	-	-
$\gamma_3$	50	0.0321 (0.0033)	94.6	-	-
	100	0.0341 (0.0031)	93.3	0.0879 (0.0033)	81.95
	150	0.0347 (0.0036)	93.4	-	-

performs very well according to this metric. It is important to note that the gains in performance are small when the sampling density is increased from 100 to 150 points. Thus, for fairly smooth functions, as is the case in this simulation and the applications presented in the subsequent section, we will sample the functions with 100 points for computational efficiency. The replicate posterior means for the proposed method are displayed in red in Figure 3(b)-(d) with the true warping in blue. It is clear from this figure that there is little variation across replicates and that we are able to recover the true warping very well.

Table 2 reports the same set of results for linear and no decay in the prior standard deviations for the proposed method across the three sampling densities. Linear decay performs comparably to quadratic decay, while no decay does not perform well as expected. Throughout the rest of the paper we utilize quadratic decay as indicated by these simulation results.

## 5.2. Simulation 2

In the second simulation, we explore the performance of the proposed alignment model when two modes are present in the posterior distribution. The two functions to be aligned,  $f_1$  and  $f_2$ , are shown in Figure 4(a) in blue and red, respectively. In the same panel, we show the alignment results, across 100 replicates, using the mean of each posterior cluster in green and black. For comparison, we also display the dynamic programming result in magenta. Note that in this simulation we have treated the number of clusters as known ( $k = 2$ ) and applied the  $k$ -means clustering algorithm. In panel (b), we display the two clusters of warping functions representing the two posterior modes (again in green and black) as well as the dynamic programming result (in magenta). The clusterwise posterior mean warping functions are much smoother than the dynamic programming solution and achieve essentially the same level of alignment between the two functions.

In Table 3 we provide a few summaries for each posterior cluster. In partic-

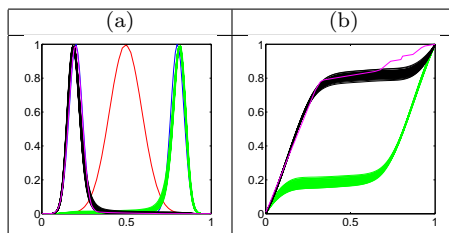


FIG 4. (a) Simulated data with  $f_1$  in blue,  $f_2$  in red,  $f_2 \circ \bar{\gamma}_1$  in green,  $f_2 \circ \bar{\gamma}_2$  in black and  $f_2 \circ \gamma_{DP}$  in magenta. (b) Estimated average warping functions in cluster 1, ( $\bar{\gamma}_1$ ) in green, in cluster 2 ( $\bar{\gamma}_2$ ) in black, and using dynamic programming ( $\gamma_{DP}$ ) in magenta.

TABLE 3

Clusterwise summaries of the posterior distribution. (a) Average cluster size. (b) Average distance between  $f_1$  and  $f_2$  after warping using the mean of each cluster. (c) Average distance between  $f_1$  and  $f_2$  after warping using the median of each cluster. (d) Average distance between  $f_1$  and  $f_2$  after warping using the MAP estimate in each cluster. The standard deviations are given in parentheses.

	(a)	(b)	(c)	(d)
Cluster 1	98.65 (6.79)	1.4890 (0.0148)	1.3688 (0.0099)	1.2931 (0.0390)
Cluster 2	101.35 (6.79)	1.4985 (0.0162)	1.3719 (0.0119)	1.3033 (0.0484)

ular, we report the average cluster size, and the average distance between the two functions based on clusterwise posterior mean, median and MAP alignment. We expect the clusters to be balanced as the peaks in the bimodal function are approximately equidistant from the peak in the unimodal function. This should also be reflected in the post-alignment, clusterwise distances between the two functions. The original distance between them is 2.6668, and the distance after dynamic programming alignment is 1.4205. The reported clusterwise distances are comparable to the dynamic programming solution when using mean warping, and better when using median and MAP warping. This shows that in addition to being able to discover multiple plausible alignments as modes of the posterior distribution, we are able to better explore the full space of warping functions than the deterministic dynamic programming algorithm.

## 6. Applications

Next, we consider pairwise alignment of functions using the proposed Bayesian model for various types of real data. We start with three types of biomedical signals: gait pressure functions, PQRST complexes extracted from electrocardiograms (ECGs) and respiration functions. For a detailed description of these datasets please see Kurtek et al. [14]. We proceed to show examples on growth velocity functions for boys and girls obtained from the Berkeley Growth Dataset (BGD) [35]. Finally, we show two examples on signature (tangential) acceleration functions from a subset of the data described in [38]. In each example, we first determine whether multiple modes exist in the posterior distribution



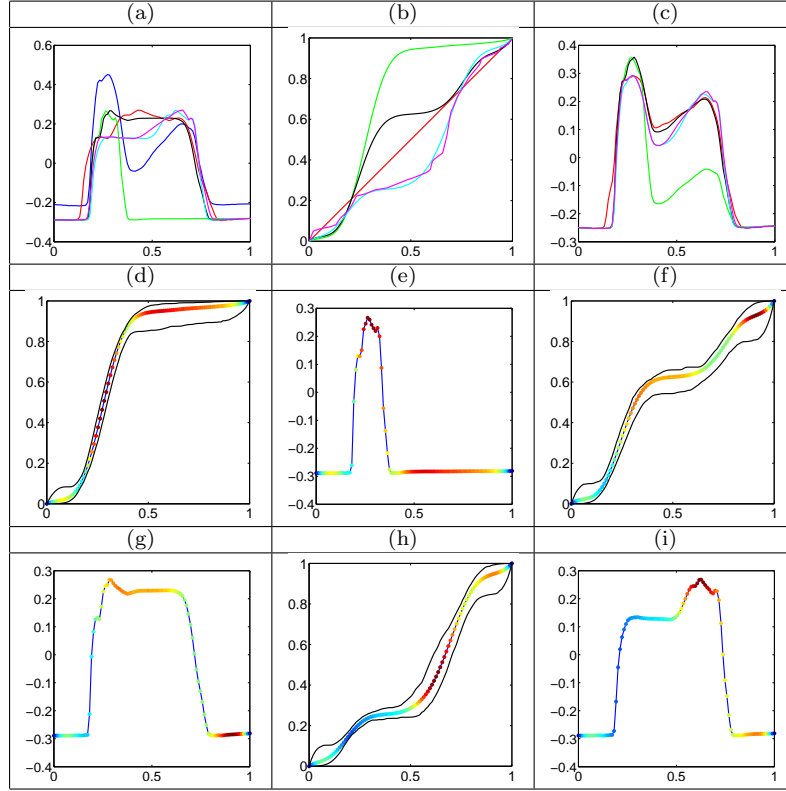


FIG 5. Pairwise alignment of two gait pressure functions. (a) Original functions  $f_1$  and  $f_2$  in blue and red, respectively.  $f_2 \circ \gamma_{DP}$  in magenta,  $f_2 \circ \bar{\gamma}_1$  in green (cluster 1),  $f_2 \circ \bar{\gamma}_2$  in black (cluster 2) and  $f_2 \circ \bar{\gamma}_3$  in cyan (cluster 3). (b)  $\gamma_{DP}$  in magenta,  $\gamma_{id}$  in red, and  $\bar{\gamma}_1$ ,  $\bar{\gamma}_2$  and  $\bar{\gamma}_3$  in green, black and cyan, respectively. (c) Pointwise average of  $f_1$  and  $f_2$  for each alignment result (colored in the same way as (a) and (b)). (d) Pointwise standard deviation (hot colors correspond to higher values) plotted on  $\bar{\gamma}_1$ , and the 95% credible interval in black. (e) Pointwise standard deviation (hot colors correspond to higher values) plotted on  $f_2 \circ \bar{\gamma}_1$ . (f)-(i) Same as (d) and (e) but for clusters 2 and 3, respectively.

of warping functions. If this is the case, we cluster the posterior samples using  $k$ -means clustering, where  $k$  is selected based on the silhouette measure [23]. Finally, we show the clusterwise alignment results and assess registration uncertainty in each cluster.

### 6.1. Biomedical Signals

First, we describe several alignment examples for biomedical signals. In all of the presented datasets, the functions must first be properly registered to align important features across the functional observations. At times, due to significant structural differences, registration ambiguities result in multiple plausible

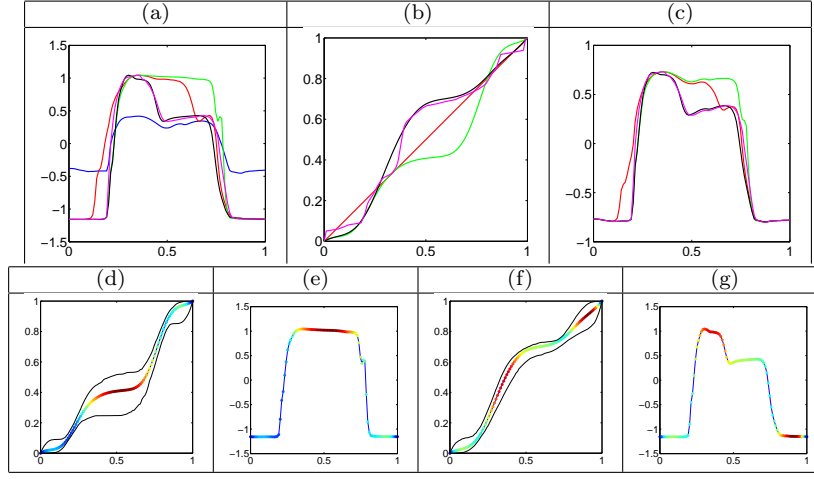


FIG 6. Pairwise alignment of two gait pressure functions. (a) Original functions  $f_1$  and  $f_2$  in blue and red, respectively.  $f_2 \circ \gamma_{DP}$  in magenta,  $f_2 \circ \bar{\gamma}_1$  in green (cluster 1) and  $f_2 \circ \bar{\gamma}_2$  in black (cluster 2). (b)  $\gamma_{DP}$  in magenta,  $\gamma_{id}$  in red, and  $\bar{\gamma}_1$  and  $\bar{\gamma}_2$  in green and black, respectively. (c) Pointwise average of  $f_1$  and  $f_2$  for each alignment result (colored in the same way as (a) and (b)). (d) Pointwise standard deviation (hot colors correspond to higher values) plotted on  $\bar{\gamma}_1$ , and the 95% credible interval in black. (e) Pointwise standard deviation (hot colors correspond to higher values) plotted on  $f_2 \circ \bar{\gamma}_1$ . (f)-(g) Same as (d)-(e) but for cluster 2.

alignments, which cannot be detected using optimization-based registration algorithms. This is especially seen in the gait pressure functional data, which we consider next.

**Gait Pressure Functions:** We begin with three examples of pairwise alignment of gait pressure functions. In the first example, shown in Figure 5, we discover three modes in the posterior distribution. Panel (a) displays the registration results using the mean warping function in each cluster. The functions to be registered are plotted in blue and red. The deterministic dynamic programming solution is given in magenta, and the three clusterwise alignments are shown in green (cluster 1), black (cluster 2) and cyan (cluster 3). The corresponding warping functions are shown in panel (b) with the identity element in red. Panel (c) displays the pointwise average of the two functions for each registration result. First, the cluster 3 alignment is nearly identical to the dynamic programming solution. The main benefit of the proposed Bayesian approach is the discovery of two other plausible alignments. The cluster 1 alignment emphasizes the first mode in the gait functions (green average in panel (c)) while the cluster 2 registration weights both modes equally (black average in panel (c)). The cluster 3 alignment as well as the dynamic programming solution emphasize both modes as well as the large dip toward the midpoint of the gait cycle. Panels (d)-(i) show the uncertainty in each cluster using two displays: (1) pointwise standard deviation as a color (blue to red=low to high) on the mean warping as well as the pointwise 95% credible interval in black, and (2) pointwise standard

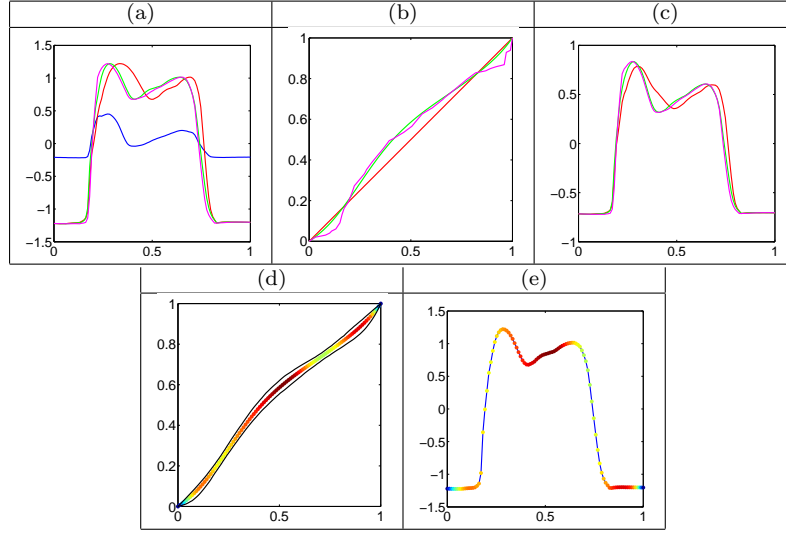


FIG 7. Pairwise alignment of two gait pressure functions. (a) Original functions  $f_1$  and  $f_2$  in blue and red, respectively.  $f_2 \circ \gamma_{DP}$  in magenta and  $f_2 \circ \bar{\gamma}$  in green. (b)  $\gamma_{DP}$  in magenta,  $\gamma_{id}$  in red, and  $\bar{\gamma}$  in green. (c) Pointwise average of  $f_1$  and  $f_2$  for each alignment result (colored in the same way as (a) and (b)). (d) Pointwise standard deviation (hot colors correspond to higher values) plotted on  $\bar{\gamma}$ , and the 95% credible interval in black. (e) Pointwise standard deviation (hot colors correspond to higher values) plotted on  $f_2 \circ \bar{\gamma}$ .

deviation as a color on the warped version of the function being registered. We usually observe lower standard deviation along the pronounced features such as the steep increase and decrease in pressure at the beginning and end of the gait cycle. On the other hand, the standard deviation is inflated in flat regions where many types of warping provide a satisfactory solution.

The second example is displayed in Figure 6. In this case, we find two modes in the posterior distribution and display the same set of results as for the first example. The results are similar as in the previous case where different modes of the pressure functions are emphasized in each cluster. Again, the cluster 2 mean is very similar to the dynamic programming solution. Importantly, the result based on the proposed Bayesian model is always much smoother while achieving very similar alignment. Finally, in Figure 7, we display an example where the posterior distribution of warping functions is unimodal. In this case, the two functions to be aligned have two very clear gait pressure modes, and thus, there is little uncertainty in the registration.

**PQRST Complexes:** The PQRST complex in electrocardiogram signals refers to the first peak (P wave), the sharp second peak (QRS complex), and the third peak (T wave). These functions have very pronounced features, and thus, most of the pairwise alignment results on this data yield a unimodal posterior distribution. We display one example of such an alignment in Figure 8. The posterior mean warping is very similar to the dynamic programming solution,

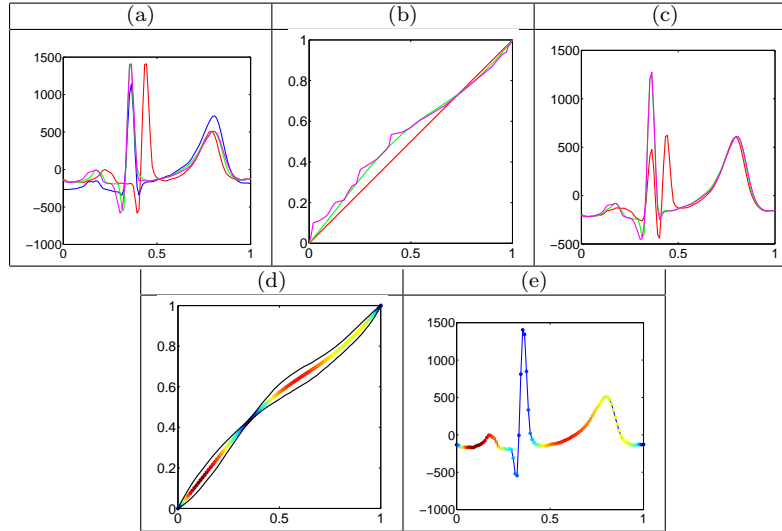


FIG 8. Pairwise alignment of two PQRST complexes. (a) Original functions  $f_1$  and  $f_2$  in blue and red, respectively.  $f_2 \circ \gamma_{DP}$  in magenta and  $f_2 \circ \tilde{\gamma}$  in green. (b)  $\gamma_{DP}$  in magenta,  $\gamma_{id}$  in red, and  $\tilde{\gamma}$  in green. (c) Pointwise average of  $f_1$  and  $f_2$  for each alignment result (colored in the same way as (a) and (b)). (d) Pointwise standard deviation (hot colors correspond to higher values) plotted on  $\tilde{\gamma}$ , and the 95% credible interval in black. (e) Pointwise standard deviation (hot colors correspond to higher values) plotted on  $f_2 \circ \tilde{\gamma}$ .

albeit smoother. Also, there is very little registration uncertainty around the QRS complex. Alignment uncertainty is also low at the T wave, which is much more pronounced than the P wave in this example. The red (no warping) pointwise average of the two PQRST complexes displayed in panel (c) is clearly not a valid PQRST complex. As a result, warping in this application is necessary to obtain reasonable functional summaries.

**Respiration Data:** Each function in this dataset represents lung volume during a breathing cycle. Respiration cycle alignment is important for understanding breathing variation as well as radiotherapy in lung cancer [14]. In this application, the posterior distribution of warping functions is also almost always unimodal due to the very simple structure of each breathing cycle. Figure 9 displays one example of pairwise alignment of two such respiration functions. Again, the produced posterior mean alignment is very good, with little uncertainty in the area of the peak of the breathing cycle.

## 6.2. Berkeley Growth Velocity Data

A major goal in studying the growth velocity functions of children is to characterize the number and timing of growth spurts in boys and girls. The BGD has been studied for these purposes before [20]. In the current paper, we emphasize that there may be multiple plausible time warpings that align growth

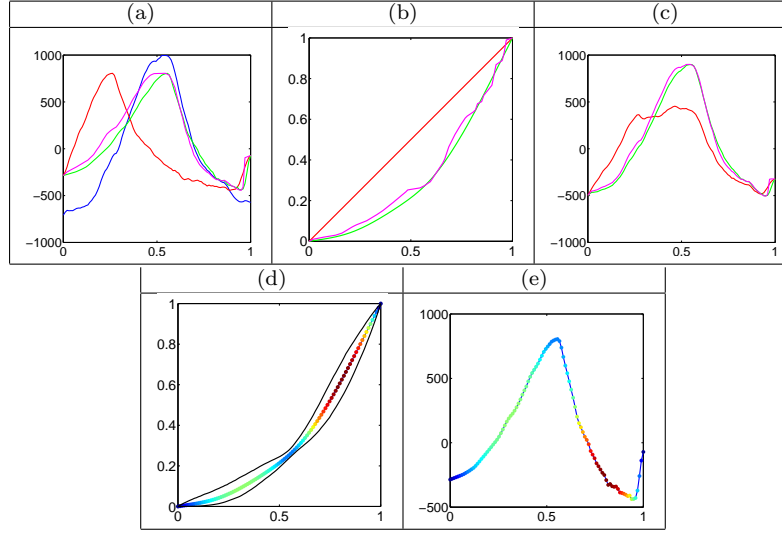


FIG 9. Pairwise alignment of two respiration functions. (a) Original functions  $f_1$  and  $f_2$  in blue and red, respectively.  $f_2 \circ \gamma_{DP}$  in magenta and  $f_2 \circ \bar{\gamma}$  in green. (b)  $\gamma_{DP}$  in magenta,  $\gamma_{id}$  in red, and  $\bar{\gamma}$  in green. (c) Pointwise average of  $f_1$  and  $f_2$  for each alignment result (colored in the same way as (a) and (b)). (d) Pointwise standard deviation (hot colors correspond to higher values) plotted on  $\bar{\gamma}$ , and the 95% credible interval in black. (e) Pointwise standard deviation (hot colors correspond to higher values) plotted on  $f_2 \circ \bar{\gamma}$ .

spurts across children. In the first example, presented in the top part of Figure 10, we examine two growth velocity functions for boys. The resulting posterior distribution on the space of warping functions is bimodal. The mean warping in both clusters nicely aligns the large growth spurt. But, the average growth velocity patterns, as seen in panel (c), are quite different depending on which alignment is used. The cluster 1 alignment (green) results in a long constant velocity growth period in the average, while cluster 2 (black) results in a decreasing velocity (at an approximately constant rate) during the same period. This presents two very different growth mechanisms, which are useful for characterizing growth functions. The second example, shown in the bottom portion of Figure 10, considers alignment of two growth velocity curves for girls. Again, we discover two modes in the posterior distribution. As seen in panel (c), the mean warping in cluster 1 (green) emphasizes the first growth spurt and is followed by a smaller second spurt. On the other hand, the mean alignment in cluster 2 results in an average growth pattern where the two growth spurts are approximately of the same size.

### 6.3. Signature Acceleration Functions

The final application considers alignment of signature acceleration functions. As described in [22, 33], each planar signature curve is first summarized using

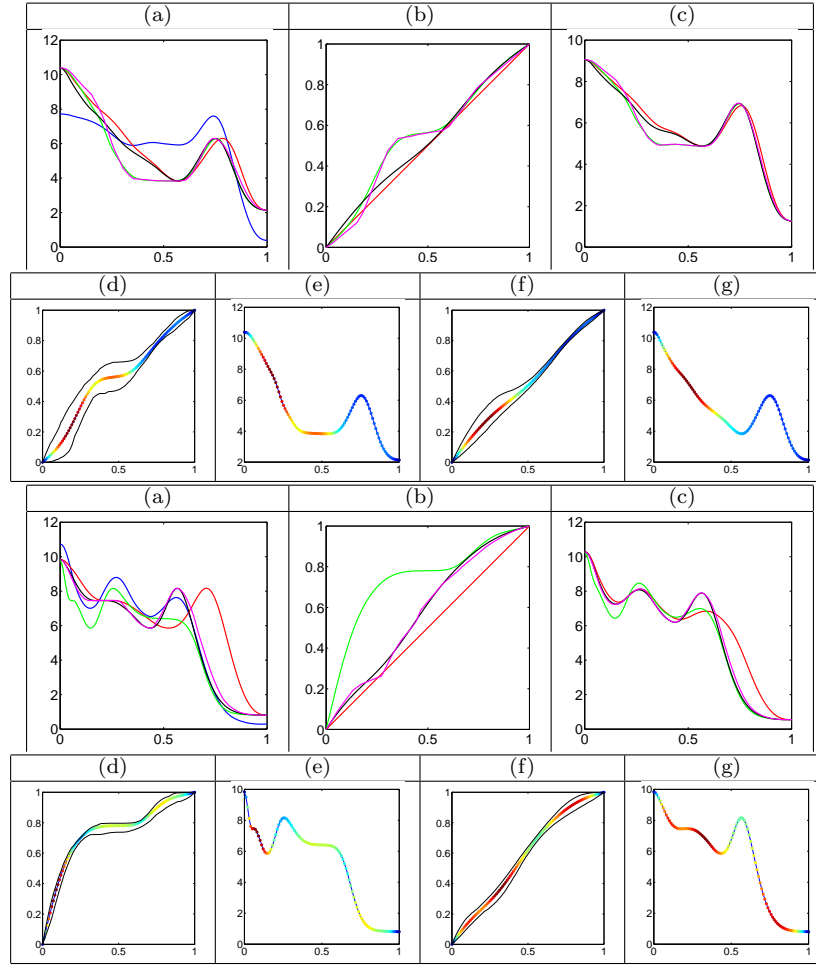


FIG 10. *Top: Pairwise alignment of two growth velocity functions for boys. Bottom: Pairwise alignment of two growth velocity functions for girls. (a) Original functions  $f_1$  and  $f_2$  in blue and red, respectively.  $f_2 \circ \gamma_{DP}$  in magenta,  $f_2 \circ \tilde{\gamma}_1$  in green (cluster 1) and  $f_2 \circ \tilde{\gamma}_2$  in black (cluster 2). (b)  $\gamma_{DP}$  in magenta,  $\gamma_{id}$  in red, and  $\tilde{\gamma}_1$  and  $\tilde{\gamma}_2$  in green and black, respectively. (c) Pointwise average of  $f_1$  and  $f_2$  for each alignment result (colored in the same way as (a) and (b)). (d) Pointwise standard deviation (hot colors correspond to higher values) plotted on  $\tilde{\gamma}_1$ , and the 95% credible interval in black. (e) Pointwise standard deviation (hot colors correspond to higher values) plotted on  $f_2 \circ \tilde{\gamma}_1$ . (f)-(g) Same as (d)-(e) but for cluster 2.*

its tangential acceleration function. Comparison and modeling of such functions are important in understanding inter and intra-class signature variability, and for signature classification. A major difficulty that arises in the analysis pipeline is that the signature acceleration functions contain natural warping variability. Thus, in order to obtain satisfactory results, such variability must be accounted for. We present two different pairwise registration results in Figures 11 and 12.

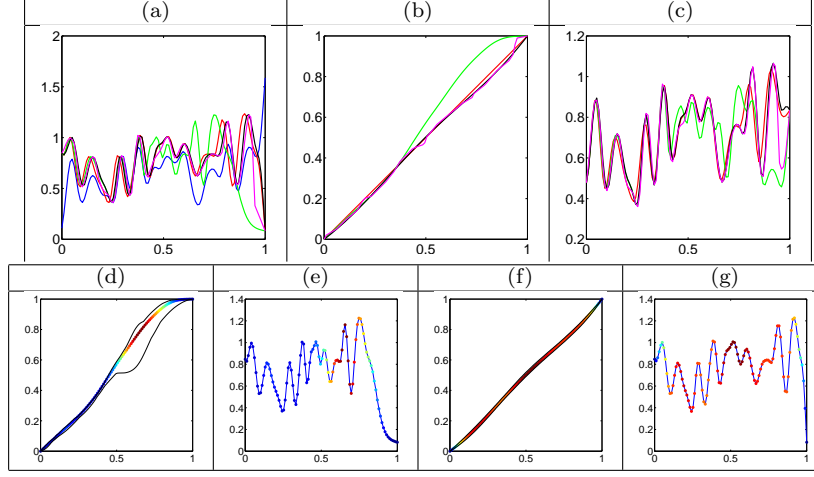


FIG 11. Pairwise alignment of two signature acceleration functions. (a) Original functions  $f_1$  and  $f_2$  in blue and red, respectively.  $f_2 \circ \gamma_{DP}$  in magenta,  $f_2 \circ \bar{\gamma}_1$  in green (cluster 1) and  $f_2 \circ \bar{\gamma}_2$  in black (cluster 2). (b)  $\gamma_{DP}$  in magenta,  $\gamma_{id}$  in red, and  $\bar{\gamma}_1$  and  $\bar{\gamma}_2$  in green and black, respectively. (c) Pointwise average of  $f_1$  and  $f_2$  for each alignment result (colored in the same way as (a) and (b)). (d) Pointwise standard deviation (hot colors correspond to higher values) plotted on  $\bar{\gamma}_1$ , and the 95% credible interval in black. (e) Pointwise standard deviation (hot colors correspond to higher values) plotted on  $f_2 \circ \bar{\gamma}_1$ . (f)-(g) Same as (d)-(e) but for cluster 2.

In the first example, the posterior distribution of warping functions contains two different modes. The posterior mean alignment agrees for close to half of the time interval at which point the mean warping in cluster 1 (green) diverges from the identity warping. This results in two drastically different alignments between the two signatures (and potentially different inferences depending on which alignment is used). Another interesting feature is that there is a large amount of uncertainty in the region where the mean warping in cluster 1 diverges from the identity element; this indicates that the corresponding region of the two acceleration functions is difficult to align. The posterior distribution in the second example is unimodal, and the posterior mean is very close to the dynamic programming solution. Furthermore, perhaps surprisingly, there is very little uncertainty in the alignment.

#### 6.4. Groupwise MAP Alignment to a Known Template

We close the applications section with several examples of groupwise function alignment to a known template. For each of the datasets described above (and an additional simulated dataset), we randomly select one of the functions in the data as a template and align all functions in a pairwise manner to this template. In these examples, we do not account for multimodality in the posterior distribution and use the maximum a posteriori (MAP) warping ( $\gamma_{MAP}$ ) for alignment.



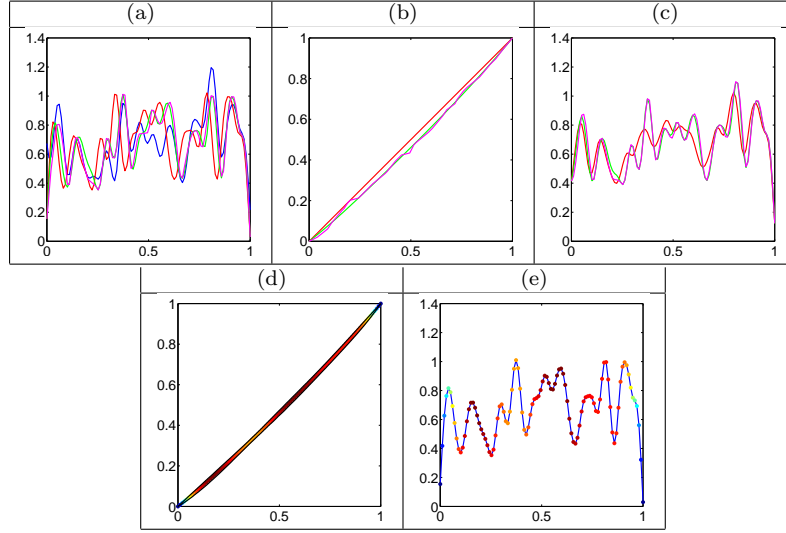


FIG 12. Pairwise alignment of two signature acceleration functions. (a) Original functions  $f_1$  and  $f_2$  in blue and red, respectively.  $f_2 \circ \gamma_{DP}$  in magenta and  $f_2 \circ \tilde{\gamma}$  in green. (b)  $\gamma_{DP}$  in magenta,  $\gamma_{id}$  in red, and  $\tilde{\gamma}$  in green. (c) Pointwise average of  $f_1$  and  $f_2$  for each alignment result (colored in the same way as (a) and (b)). (d) Pointwise standard deviation (hot colors correspond to higher values) plotted on  $\tilde{\gamma}$ , and the 95% credible interval in black. (e) Pointwise standard deviation (hot colors correspond to higher values) plotted on  $f_2 \circ \tilde{\gamma}$ .

The results are presented in Figures 13 and 14. For each example, we display the full original dataset with the template highlighted in black in panel (a). We show the aligned data in panel (b), the pointwise function averages before (red) and after (green) alignment in panel (c), and the estimated warping functions in panel (d). In all examples, we see a drastic improvement in function alignment using the proposed method, which directly translates to better data summaries such as the pointwise function averages. As a specific example, consider the PQRS complexes in row (3). The MAP alignment is able to correctly match the P waves, QRS complexes and T waves across all of the given data. This results in an accurate representation of the pointwise average, which shares all of the features present in the original data. On the other hand, the QRS complex is highly distorted in the unaligned pointwise average. Similar results are observed in the other examples with highest improvement for the gait pressure data and the signature acceleration data.

## 7. Summary and Future Work

We have presented a Bayesian model for pairwise registration of functional data. This model utilizes a convenient geometric representation of warping functions called the square-root density, which allows for efficient sampling from the posterior distribution via importance sampling. A main advantage of the proposed

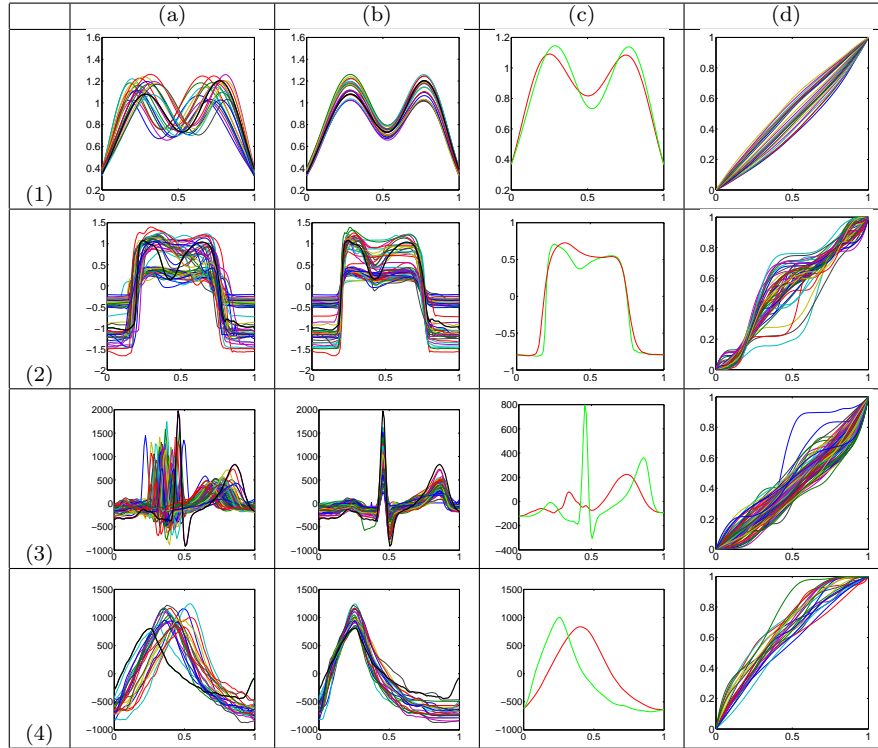


FIG 13. Groupwise maximum a posteriori alignment to a known template. (a) Original functions with the template in black. (b) Aligned functions  $(f \circ \gamma_{MAP})$  with the template in black. (c) Pointwise average before (red) and after alignment (green). (d) Warping functions  $\gamma_{MAP}$ . (1) Simulated data. (2) Gait data. (3) PQRST complex data. (4) Respiration data.

approach over previous optimization-based approaches is that it is possible to discover multiple plausible registrations, which are given by different modes in the posterior distribution. We present several simulated and real data examples that highlight these advantages. We use simulations to compare the results obtained using the proposed model to those obtained using a similar model with a Dirichlet process prior on the warping functions (which does not exploit the geometry of the space of warping functions).

In future work, we will extend these methods to a groupwise registration algorithm where the template functions and the warping functions are jointly estimated. Furthermore, we will extend these methods to a setting where soft landmark information is provided on the functions of interest. In such a case, one can incorporate this information into the prior distribution of the Bayesian model. Finally, we will consider a more general problem of curve alignment for shape analysis where the curves are functions from a unit interval (open curves) or unit circle (closed curves) to  $\mathbb{R}^n$ ,  $n > 1$ . Shapes of objects are invariant to translation, scale, rotation and re-parameterization, and thus, the prior distribu-

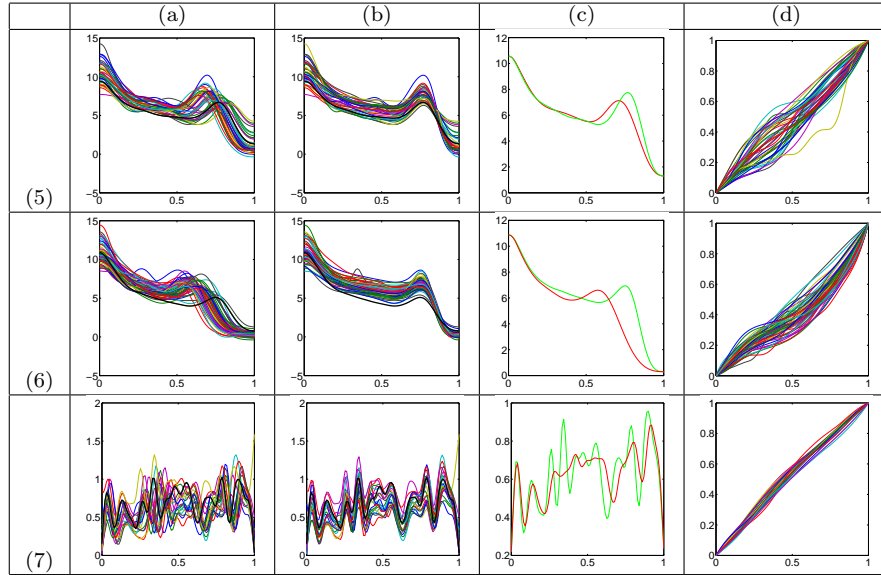


FIG 14. Groupwise maximum a posteriori alignment to a known template. (a) Original functions with the template in black. (b) Aligned functions ( $f \circ \gamma_{MAP}$ ) with the template in black. (c) Pointwise average before (red) and after alignment (green). (d) Warping functions  $\gamma_{MAP}$ . (5) BGD for boys. (6) BGD for girls. (7) Signature acceleration data.

tions in our Bayesian model will be defined on product spaces, whose geometric structure will play an important role.

### Acknowledgements

The author would like to thank Anuj Srivastava and Karthik Bharath for useful suggestions and comments.

### References

- [1] BHATTACHARYA, A. (1943). On a measure of divergence between two statistical populations defined by their probability distributions. *Bulletin of the Calcutta Mathematical Society* **35** 99-109.
- [2] CHENG, W., DRYDEN, I. L., HITCHCOCK, D. B., HUANG, X. and LE, H. (2013). Bayesian registration of functions and curves. *Bayesian Analysis* doi: 10.1214/15-BA957.
- [3] COTTER, S. L., ROBERTS, G. O., STUART, A. M. and WHITE, D. (2013). MCMC Methods for Functions: Modifying Old Algorithms to Make Them Faster. *Statistical Science* **28** 424-446.
- [4] DRYDEN, I. L. (2005). Statistical analysis on high-dimensional spheres and shape spaces. *Annals of Statistics* **33** 1643-1665.

- [5] DRYDEN, I. L. and MARDIA, K. V. (1998). *Statistical Shape Analysis*. John Wiley & Sons.
- [6] FLETCHER, P. T., VENKATASUBRAMANIAN, S. and JOSHI, S. (2009). The geometric median on Riemannian manifolds with application to robust atlas estimation. *Neuroimage* **45** S143–S152.
- [7] GERVINI, D. and GASSER, T. (2004). Self-Modeling Warping Functions. *Journal of the Royal Statistical Society, Series B* **66** 959–971.
- [8] JAMES, G. (2007). Curve Alignment by Moments. *Annals of Applied Statistics* **1** 480–501.
- [9] KNEIP, A. and GASSER, T. (1992). Statistical Tools to Analyze Data Representing a Sample of Curves. *Annals of Statistics* **20** 1266–1305.
- [10] KNEIP, A. and RAMSAY, J. O. (2008). Combining Registration and Fitting for Functional Models. *Journal of the American Statistical Association* **103** 1155–1165.
- [11] KURTEK, S., SRIVASTAVA, A., KLASSEN, E. and DING, Z. (2012). Statistical Modeling of Curves Using Shapes and Related Features. *Journal of the American Statistical Association* **107** 1152–1165.
- [12] KURTEK, S., SRIVASTAVA, A. and WU, W. (2011). Signal estimation under random time-warpings and nonlinear signal alignment. In *Neural Information Processing Systems (NIPS)* 675–683.
- [13] KURTEK, S., SU, J., GRIMM, C., VAUGHAN, M., SOWELL, R. T. and SRIVASTAVA, A. (2013). Statistical Analysis of Manual Segmentations of Structures in Medical Images. *Computer Vision and Image Understanding* **117** 1036–1050.
- [14] KURTEK, S., WU, W., CHRISTENSEN, G. E. and SRIVASTAVA, A. (2013). Segmentation, alignment and statistical analysis of biosignals with application to disease classification. *Journal of Applied Statistics* **40** 1270–1288.
- [15] LE, H. (2001). Locating Frechet Means with Application to Shape Spaces. *Advances in Applied Probability* **33** 324–338.
- [16] LIU, X. and MÜLLER, H. G. (2004). Functional convex averaging and synchronization for time-warped random curves. *Journal of the American Statistical Association* **99** 687–699.
- [17] MACQUEEN, J. B. (1967). Some Methods for Classification and Analysis of MultiVariate Observations. In *Fifth Berkeley Symposium on Mathematical Statistics and Probability* (L. M. L. CAM and J. NEYMAN, eds.) **1** 281–297.
- [18] MARRON, J. S., RAMSAY, J. O., SANGALLI, L. M. and SRIVASTAVA, A. (2014). Statistics of time warpings and phase variations. *Electronic Journal of Statistics* **8** 1697–1702.
- [19] RAKET, L. L., SOMMER, S. and MARKUSSEN, B. (2014). A nonlinear mixed-effects model for simultaneous smoothing and registration of functional data. *Pattern Recognition Letters* **38** 1 - 7.
- [20] RAMSAY, J. O., BOCK, R. D. and GASSER, T. (1995). Comparison of height acceleration curves in the Fels, Zurich, and Berkeley growth data. *Annals of Human Biology* **22** 413–426.
- [21] RAMSAY, J. O. and LI, X. (1998). Curve Registration. *Journal of the Royal Statistical Society, Series B* **60** 351–363.

- [22] RAMSAY, J. O. and SILVERMAN, B. W. (2005). *Functional Data Analysis, Second Edition*. Springer Series in Statistics.
- [23] ROUSSEEUW, P. (1987). Silhouettes: A Graphical Aid to the Interpretation and Validation of Cluster Analysis. *Journal of Computational and Applied Mathematics* **20** 53–65.
- [24] SKARE, O., BOLVIKEN, E. and HOLDEN, L. (2003). Improved Sampling-Importance Resampling and Reduced Bias Importance Sampling. *Scandinavian Journal of Statistics* **30** 719–737.
- [25] SRIVASTAVA, A., JERMYN, I. and JOSHI, S. H. (2007). Riemannian Analysis of Probability Density Functions with Applications in Vision. In *IEEE Conference on Computer Vision and Pattern Recognition (CVPR)* 1–8.
- [26] SRIVASTAVA, A., KLASSEN, E., JOSHI, S. H. and JERMYN, I. H. (2011). Shape Analysis of Elastic Curves in Euclidean Spaces. *IEEE Transactions on Pattern Analysis and Machine Intelligence* **33** 1415–1428.
- [27] SRIVASTAVA, A., WU, W., KURTEK, S., KLASSEN, E. and MARRON, J. S. (2011). Registration of Functional Data Using Fisher-Rao Metric. *arXiv:1103.3817v2*.
- [28] SUEMATSU, N. and HAYASHI, A. (2012). Time series alignment with Gaussian processes. In *IEEE International Conference on Pattern Recognition (ICPR)* 2355–2358.
- [29] TANG, R. and MÜLLER, H. G. (2008). Pairwise curve synchronization for functional data. *Biometrika* **95** 875–889.
- [30] TELESKA, D. and INOUE, L. Y. T. (2008). Bayesian hierarchical curve registration. *Journal of the American Statistical Association* **103** 328–339.
- [31] TELESKA, D., INOUE, L. Y. T., NEIRA, M., ETZIONI, R., GLEAVE, M. and NELSON, C. (2009). Differential Expression and Network Inferences through Functional Data Modeling. *Biometrics* **65** 793–804.
- [32] TSAI, T. H., TADESSE, M. G., WANG, Y. and RESSOM, H. W. (2013). Profile-Based LC-MS Data Alignment: A Bayesian Approach. *IEEE/ACM Transactions on Computational Biology and Bioinformatics* **99** 494–503.
- [33] TUCKER, J. D., WU, W. and SRIVASTAVA, A. (2013). Generative models for functional data using phase and amplitude separation. *Computational Statistics & Data Analysis* **61** 50–66.
- [34] TUCKER, J. D., WU, W. and SRIVASTAVA, A. (2014). Analysis of signals under compositional noise with applications to SONAR data. *IEEE Journal of Oceanic Engineering* **39** 318–330.
- [35] TUDDENHAM, R. D. and SNYDER, M. M. (1954). Physical growth of California boys and girls from birth to eighteen years. *Publications in child development. University of California, Berkeley* **1** 183.
- [36] ČENCOV, N. N. (1982). *Statistical Decision Rules and Optimal Inferences. Translations of Mathematical Monographs* **53**. AMS, Providence, USA.
- [37] WU, W. and SRIVASTAVA, A. (2011). An information-geometric framework for statistical inferences in the neural spike train space. *Journal of Computational Neuroscience* **31** 725–748.
- [38] YEUNG, D., CHANG, H., XIONG, Y., GEORGE, S., KASHI, R., MATSUMOTO, T. and RIGOLL, G. (2004). SVC2004: First international sig-

nature verification competition. In *International Conference on Biometric Authentication (ICBA)* 16–22.